THE JOURNAL OF PHYSICAL CHEMISTRY A
A JOURNAL OF THE AMERICAN CHEMICAL SOCIETY

pubs.acs.org/JPCA Article

Probing Hydrogen-Bonding Interactions within Phenol-Benzimidazole Proton-Coupled Electron Transfer Model Complexes with Cryogenic Ion Vibrational Spectroscopy

Liangyi Chen and Joseph A. Fournier*

Cite This: *J. Phys. Chem. A* 2021, 125, 9288−9297 Read Online

ACCESS | Metrics & More | Article Recommendations | Supporting Information

ABSTRACT: Hydrogen-bonding interactions within a series of phenol-benzimidazole model proton-coupled electron transfer (PCET) dyad complexes are characterized using cryogenic ion vibrational spectroscopy. A highly red-shifted and surprisingly broad (>1000 cm^{-1}) transition is observed in one of the models and assigned to the phenolic OH stretch strongly H-bonded to the $N_{(3)}$ benzimidazole atom. The breadth is attributed to a combination of anharmonic Fermi-resonance coupling between the OH stretch and background doorway states involving OH bending modes and strong coupling of the OH stretch frequency to structural deformations along the proton-transfer coordinate accessible at the vibrational zero-point level. The other models show unexpected protonation of the benzimidazole group upon electrospray ionization instead of at more basic remote amine/amide groups. This leads to the formation of HO−$^{+}$HN$_{(3)}$ H-bond motifs that are much weaker than the OH−$N_{(3)}$ H-bond arrangement. H-bonding between the $N_{(1)}H^{+}$ benzimidazole group and the carbonyl on the tyrosine backbone is the stronger and preferred interaction in these complexes. The results show that conjugation effects, secondary H-bond interactions, and H-bond soft modes strongly influence the OH−$N_{(3)}$ interaction and highlight the importance of the direct monitoring of proton stretch transitions in characterizing the proton-transfer reaction coordinate in PCET systems.

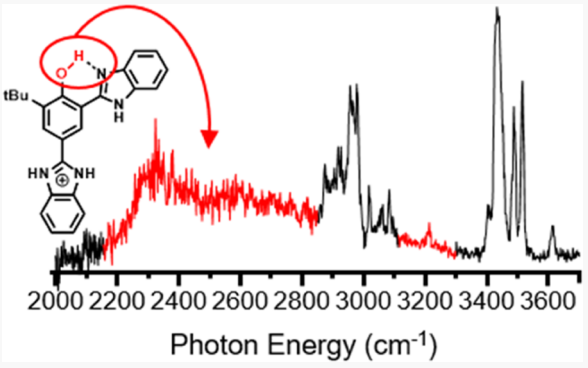

INTRODUCTION

Proton-coupled electron transfer (PCET) reactions are vitally important in biological and chemical catalysis, where the concerted transfer of a proton and electron from a common donor group to different acceptor groups via a single transition state avoids the formation of high-energy intermediates.[1,2] Perhaps the best-known example occurs during photosynthesis, where photo-oxidized chlorophyll $P680^{\bullet+}$ in Photosystem II is reduced via the oxidation of water by the oxygen-evolving complex.[3,4] A key component in this process is the tyrosine Z (Tyr_Z) residue that directly reduces $P680^{\bullet+}$. Electron transfer from Tyr_Z to $P680^{\bullet+}$ is accompanied by the concerted transfer of the phenolic proton to the imidazole moiety of the nearby histidine 190 (His_{190}) residue. The Tyr_Z−His_{190} pair is strongly H-bonded with a very short proton donor−acceptor distance, d_{ON}, of 2.5 Å.[5] The oxidized Tyr_Z is then reduced by electron transfer from the oxygen-evolving complex. This process occurs during each of the four photoexcitation events of the Kok cycle.

Owing to the central importance of the Tyr_Z−His_{190} pair to photosynthetic water oxidation, numerous model systems have been developed and investigated with a variety of solution-phase techniques.[6−16] The most popular models are phenol-benzimidazole and phenol-pyridine dyad complexes appended to a photoexcitable group whose electronic excitation initiates PCET. A main aim in many of these studies was to determine and quantify how structural factors influence PCET rates, specifically d_{ON} and the reaction driving force ΔG^0 (largely governed by ΔpK_a between proton donor and acceptor). Although these studies have provided impressive insight and greatly improved our understanding of PCET, they have also raised many more fundamental questions. For example, early studies suggested driving force to be the most important factor,[6] while later studies concluded d_{ON} to be the crucial parameter.[8,17] In some systems, H-bond soft mode vibrations have been shown to be critically important in promoting PCET,[17−21] while other systems display temperature-independent PCET rates,[10,22] even at cryogenic temperatures, indicating facile tunneling of both electron and proton without the need for soft mode "vibrational enhancement". A wide range of kinetic isotope effects have been measured, including

Received: July 1, 2021
Revised: October 5, 2021
Published: October 15, 2021

https://doi.org/10.1021/acs.jpca.1c05879
J. Phys. Chem. A 2021, 125, 9288−9297

1 (interpreted as evidence for step-wise electron transfer followed by proton transfer)[12] and even <1 (indicating transfer to vibrationally excited acceptor states where the overlap of the deuteron wave functions are greater than those of the proton).[12,17] A very recent report employing ultrafast two-dimensional electronic-vibrational spectroscopy concluded that large structural and solvent rearrangements are necessary for the charge transfers to occur.[16]

The high degree of sensitivity and variation of measured PCET rates in solution to structural and dynamical factors[23,24] demonstrates the need for a more systematic, controlled approach for the interrogation of the key components that most influence PCET reactions. Further, solution-phase spectroscopic experiments to date have exclusively focused on the electron transfer half of PCET by monitoring, for example, the recovery of the electronic ground-state transition of the appended photoexcitable group (e.g., $Ru(bpy)_3^{2+}$). The proton-transfer component has only been inferred through kinetic isotope effects, the appearance of fingerprint vibrations associated with transfer to the base,[16] or frequency shifts of a vibrational probe group.[25] Proton stretching vibrations have yet to be monitored and, thus, direct interrogation of the proton-transfer reaction coordinate remains unexplored.

Cryogenic ion vibrational spectroscopy (CIVS) has proven to be a highly versatile method for the study of increasingly complex chemical systems isolated from solution and prepared in a composition-selected fashion using mass spectrometric approaches.[26−28] Isolation of the desired chemical system removes many of the difficulties encountered in the solution phase, such as working with complicated heterogeneous mixtures, strong solvent background, and the role/choice of solvent. Cryogenic cooling freezes the ions into well-defined minimum-energy structures, allowing for the collection of well-resolved optical action spectra that afford robust structure determination. CIVS has been invaluable in the study of strong H-bonding interactions, which often manifest as broad proton stretching transitions[29−34] and remain incredibly challenging to study directly in solution using ultrafast infrared spectroscopies.[35−38] CIVS, therefore, presents itself as an ideal approach for the study of model PCET systems and, importantly, direct interrogation of the proton-transfer reaction coordinate.

Here, we present the ground electronic state cryogenic ion vibrational spectra for the series of phenol-benzimidazole dyad complexes labeled (**1**)−(**6**) in Figure 1. Compound (**3**) shows a highly red-shifted phenolic OH stretch with a maximum near 2300 cm^{-1}, indicating a very strong H-bond with the benzimidazole $N_{(3)}$ atom (see numbering scheme, Figure 1). The OH stretch transition is surprisingly broad, spanning 2100−3300 cm^{-1}. The breadth of the H-bonded OH stretch in (**3**) is attributed to a combination of anharmonic coupling to background doorway states and sensitivity of the OH stretch frequency to heavy-atom displacements along the proton-transfer coordinate. Interestingly, spectra from all other compounds display non-H-bonded OH stretches and are consistent with protonation of the benzimidazole $N_{(3)}$ position, despite the presence of much more basic amine groups. These compounds display signatures of a weak $HO-{}^{+}HN_{(3)}$ H-bonding interaction, and, in fact, the preferred interaction is the formation of a relatively strong H-bond between the $N_{(1)}H^{+}$ group and the carbonyl group on the tyrosine backbone. The experimental results provide an important benchmark for modeling and understanding the multidimensional electronic ground-state proton-transfer potential energy surface from which PCET is initiated and raise new questions regarding the role and influence of secondary interactions on the proton-transfer coordinate.

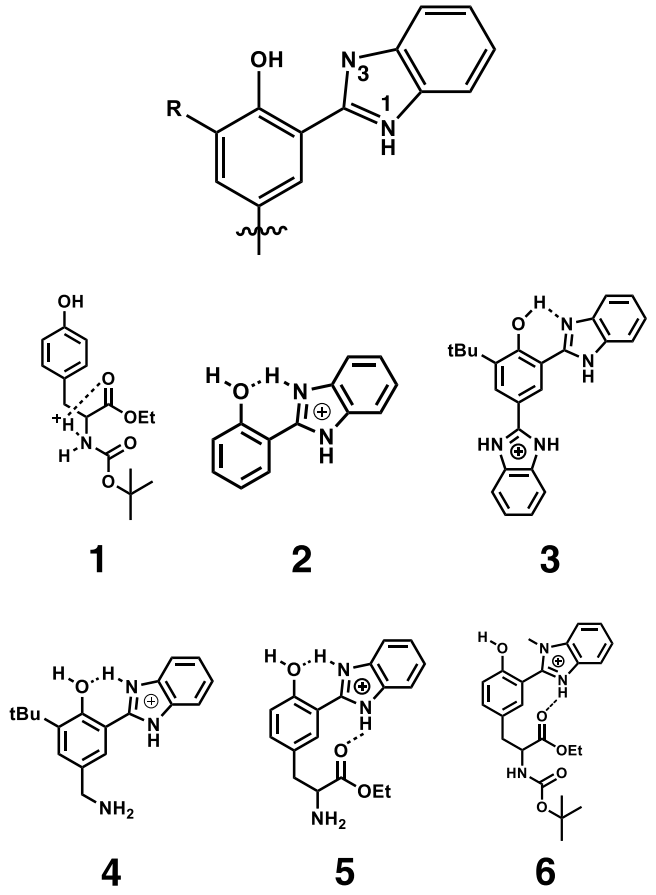

Figure 1. Top: Phenol-benzimidazole PCET model dyad scaffold and benzimidazole numbering scheme. R = H or *tert*-butyl. (**1**)−(**6**): Models studied and characterized here using cryogenic ion vibrational spectroscopy.

METHODS

The model compounds were synthesized according to literature protocols, the details of which are given in the Supporting Information along with NMR characterization.

The experiments were performed using a home-built photofragmentation mass spectrometer similar to those of Johnson[39] and Garand.[40] Briefly, ions were generated by electrospray from ∼200 μM samples in methanol with a trace amount of formic acid. Deuterium exchange was accomplished by preparing solutions with CD_3OD and purging the electrospray source with a stream of dry compressed air. The generated ions were guided through three differentially pumped stages using RF-only hexapole ion guides. The ions were cryogenically cooled in a Paul trap (Jordan TOF) attached to a closed-cycle helium cryostat. Helium buffer gas was introduced through a pulse valve to trap and collisionally cool the ions. The ion trap was held at 28 K and conditions were optimized for the condensation of a single N_2 messenger tag onto the ions. Untagged parent ions were swept out of the trap by applying a low-amplitude RF pulse tuned to the secular frequency of the untagged ion.[29] The tagged ions and photofragments were extracted into the time-of-flight region

https://doi.org/10.1021/acs.jpca.1c05879
J. Phys. Chem. A 2021, 125, 9288−9297

by pulsing the exit electrode of the Paul trap to −400 V. Extraction optics were floated at −1500 V. A dual-stage reflectron focused the ions onto a dual MCP detector.

Tunable IR light was generated in an optical parametric oscillator/amplifier (OPO/OPA) system (LaserVision) pumped by a Nd:YAG laser (Continuum Surelite EX, 10 Hz, 7 ns, 660 mJ/pulse). The output of the OPO/OPA is tunable from 2000 to 4500 cm^{-1} with pulse energies spanning 2−40 mJ/pulse. The lower-frequency range (600−2200 cm^{-1}, 0.1−1 mJ/pulse) was generated through difference frequency mixing of the OPA signal and idler beams in $AgGaSe_2$. The resolution is estimated to be 3−6 cm^{-1}. The output was focused directly into the ion trap through a KBr window after the mass-selective sweeping pulse. Tag-loss photofragmentation was recorded as a function of the scanned laser frequency to give linear action spectra. Reported spectra are averages of 16−26 scans binned by 1 cm^{-1}. Spectra were normalized by dividing by the laser power at each frequency to take into account large variations in laser power over the tuning range. Spectra in the higher-frequency region were collected at reduced laser powers to ensure linearity.

Quantum chemical calculations were performed with Gaussian09[41] at the B3LYP/6-311+G(d,p) level of theory and basis set. Scaling factors of ∼0.96 were used to scale harmonic frequency calculations in the high-frequency region (2200−3700 cm^{-1}) to bring the predicted free OH or NH stretches into an agreement with the measured frequencies. Harmonic spectra in the lower-frequency region (1200−1700 cm^{-1}) were scaled by 0.99 to bring the highest energy transitions predicted in that region in line with those observed.

RESULTS

Optimized structures, relative energies, and harmonic vibrational spectra for several possible conformers and/or protonation isomers of each model compound are given in the Supporting Information, Figures S1−S6. Parameters that are most critical to the proton-transfer coordinate (d_{ON}, d_{OH}, COH angle, CNH angle, and dihedral twist between the phenol and benzimidazole rings) are also reported in the SI for each minimum-energy structure. While the spectra presented are largely consistent with the computed minimum-energy structures, the observed transitions and their evolution between different models allow for a self-consistent set of assignments.

Compounds (1)−(3). The N_2-predissociation vibrational spectra of (**1**)−(**3**) are shown in Figure 2. Compound (**1**), tyrosine ethyl ester with a BOC protecting group, establishes the frequency of a non-H-bonded phenolic OH stretch, which is observed at 3645 cm^{-1} (Figure 2a). Three nearly isoenergetic structures were found computationally (Figure S1): two with protonation of the amide group and one with protonation of the BOC carbonyl. Although protonation of the BOC carbonyl is predicted to be lowest in energy when accounting for zero-point energy corrections (by ∼200 cm^{-1}), the computed vibrational spectrum of this isomer is not consistent with the experimental spectrum. Instead, the spectrum is most consistent with protonation at the amide nitrogen to form a $-NH_2^+$ moiety. The broad feature centered near 2500 cm^{-1} is assigned to a NH^+ amide stretch arising from a strong ionic H-bond with the neighboring ethyl ester carbonyl (see computed structures, Figure S1). The appearance of this feature is similar in frequency and breadth to the NH^+ stretch observed in protonated *N*-methylglycine-glycine,

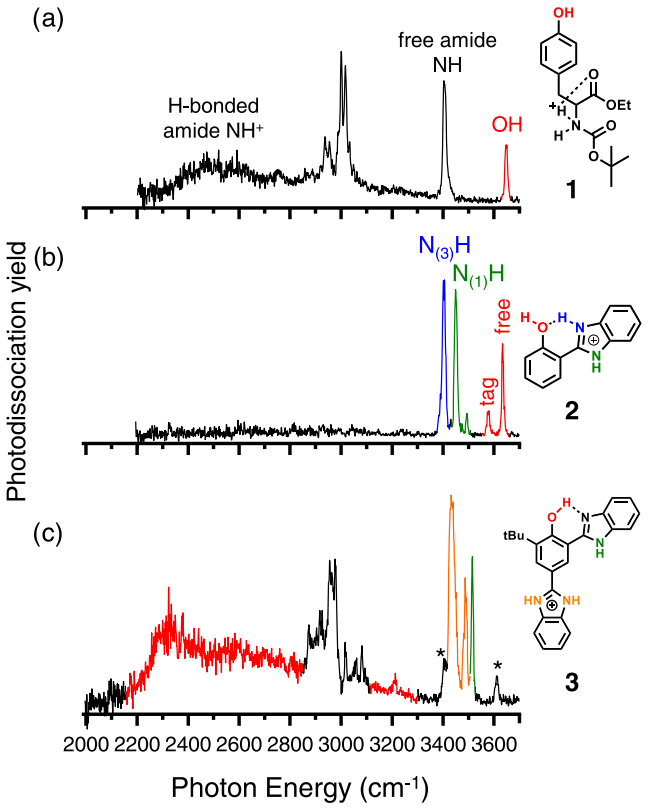

Figure 2. Cryogenic ion vibrational spectra of (a) model (**1**), (b) model (**2**), and (c) model (**3**). The non-H-bonded OH stretch (red) in (**1**) splits into a doublet in (**2**) due to isomers arising from different N_2-tag binding sites. The formation of a strong OH−$N_{(3)}$ H-bond in (**3**) yields a highly red-shifted and broad OH stretch transition. The weakly H-bonded $N_{(3)}H$ stretch in (**2**) is shown in blue, while the $N_{(1)}H$ stretch in (**2**) and (**3**) is colored green. The asterisks in (c) denote transitions arising from an isomer where protonation occurs at the $N_{(3)}$ position of the *ortho* benzimidazole moiety.

where the protonated terminal $-NH_2^+$ amide forms a strong ionic H-bond with its neighboring carbonyl.[34] The transition at 3405 cm^{-1}, then, is assigned to a non-H-bonded NH stretch of the amide group. The CH stretch region near 3000 cm^{-1} is dominated by BOC and ethyl-derived transitions, which are predicted to be much more intense than aromatic CH stretches.

Figure 2b shows the vibrational spectrum of (**2**), a simple dyad with benzimidazole appended to the *ortho* position of phenol. Compound (**2**) has only one plausible protonation site, the benzimidazole $N_{(3)}$ atom, and provides the baseline example of an HO−$^+HN_{(3)}$ H-bond. As anticipated, a free phenolic OH stretch is observed near 3633 cm^{-1}. The red shift of the OH stretch compared to that in (**1**) is likely a consequence of weakening of the OH bond due to increased π-electron conjugation from the addition of the appended benzimidazole. The free OH stretch is accompanied by a weaker partner at 3576 cm^{-1} assigned to an isomer, where the N_2 tag binds to the OH group. Three NH stretch transitions are observed: 3402, 3450, and 3493 cm^{-1}. The weak transition at 3493 cm^{-1} is assigned to the $N_{(1)}H^+$ stretch of the OH-tag-bound isomer and is about 20 cm^{-1} red-shifted of the $N_{(1)}H$ stretch in gas-phase neutral benzimidazole.[42] The two stronger transitions, therefore, derive from a tag-bound $N_{(1)}H^+$ stretch and the $N_{(3)}H^+$ stretch. The consistent ∼50 cm^{-1} tag splitting

https://doi.org/10.1021/acs.jpca.1c05879
J. Phys. Chem. A 2021, 125, 9288−9297

observed throughout the model series points to the 3450 cm^{-1} transition deriving from the tag-perturbed $N_{(1)}H^+$ stretch. This leaves the 3402 cm^{-1} feature to be assigned to the $N_{(3)}H^+$ stretch, a red shift of about 100 cm^{-1} upon H-bonding to the phenolic O atom compared to the free, non-tag-bound $N_{(1)}H^+$ stretch. The transition remains quite sharp, however, with a full width at half-maximum of 15 cm^{-1}.

Finally, the vibrational spectrum for (**3**) is given in Figure 2c. This compound contains benzimidazole groups at the *ortho* and *para* positions of the phenol ring with an added *tert*-butyl group at the second *ortho* position. The most striking feature is the low-energy, broad transition peaked near 2300 cm^{-1}. The onset of the transition is relatively sharp, starting near 2100 cm^{-1} and extending through the CH stretch region to approximately 3300 cm^{-1}. Although difficult to discern at the level of noise, some substructure is evident within the band. The calculated d_{ON} donor−acceptor distance is 2.53 Å, and the scaled harmonic frequency is 2690 cm^{-1}, both indicative of a very strong OH−$N_{(3)}$ H-bond interaction (scaling factor of 0.957 to bring the predicted *ortho* $N_{(1)}H$ stretch into an agreement with the experimentally observed transition; Figure S3). The sharp transition at 3513 cm^{-1} (green, Figure 2c) derives from the $N_{(1)}H$ stretch of *ortho* benzimidazole, matching the observed $N_{(1)}H$ stretch in gaseous neutral benzimidazole.[42] The pair of transitions at 3435 and 3487 cm^{-1} (orange, Figure 2c) then derive from the protonated *para* benzimidazole. Harmonic calculations (Figure S3) predict a closely spaced (∼10 cm^{-1}) doublet arising from two mainly localized NH^+ stretches, but the larger observed splitting and greater breadth of the lower-frequency transition suggest that the pair result from one tag-shifted and one free NH^+ stretch, respectively. There is, in addition, a weak transition near 3610 cm^{-1} consistent with a non-H-bonded phenolic OH stretch. There is also a weak shoulder at 3400 cm^{-1} in a similar location to where the H-bonded $N_{(3)}H^+$ stretch was observed in (**2**). Two constitutional isomers, therefore, appear to be present: one with protonation at the *para* benzimidazole and one with protonation at the *ortho* benzimidazole. The intensities of the transitions indicate that the dominate isomer is the former. Importantly, the presence of the latter isomer does not hinder the analysis of the OH−$N_{(3)}$ interaction.

Compounds (4)−(6). The spectrum of (**2**) is reproduced in Figure 3a, while those of (**4**)−(**6**) are given in Figure 3b−d, respectively. All spectra are consistent with protonation of the benzimidazole group and not the more basic amine/amide groups. Harmonic calculations for each of these species do indeed predict protonated benzimidazole isomers to be lowest in energy (Supporting Information).

Compound (**4**) includes a *tert*-butyl group at the second *ortho* position to the OH group and an ethyl amine group in the *para* position. Like (**2**), there are two OH stretch transitions at 3610 and 3679 cm^{-1} with the lower-frequency transition corresponding to an isomer where N_2 binds to OH. The free, untagged OH stretch of (**4**) is the most blue-shifted of all of the compounds likely due to the presence of steric effects from the bulky *tert*-butyl group. Two NH stretches are observed at 3440 and 3485 cm^{-1} assigned to the H-bonded $N_{(3)}H^+$ (blue) and free $N_{(1)}H^+$ (green) stretches, respectively. No amine NH_2 stretches are observed, which are predicted to be quite weak and nearly degenerate with benzimidazole NH stretches (Figure S4).

Compound (**5**) is tyrosine ethyl ester with benzimidazole attached at the *ortho* position. The OH stretch region again

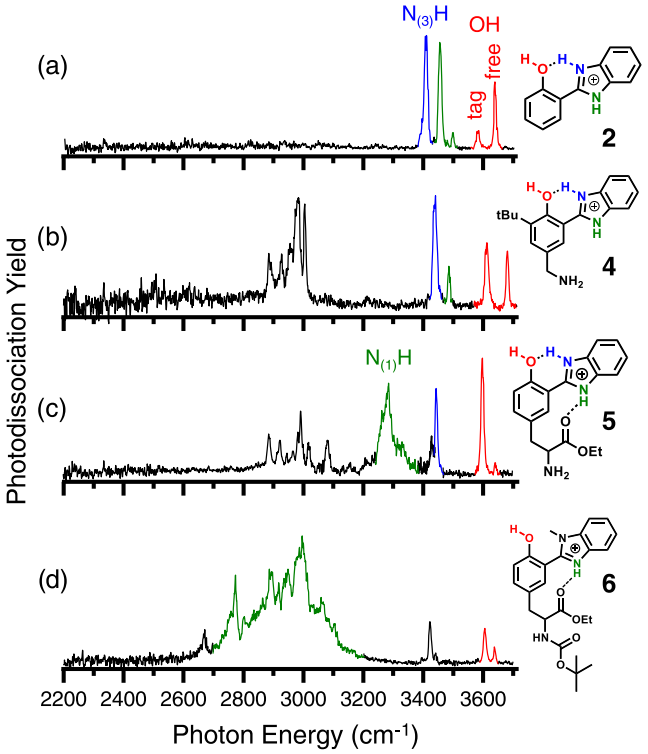

Figure 3. Cryogenic ion vibrational spectra of (a) model (**2**), (b) model (**4**), (c) model (**5**), and (d) model (**6**). Protonation occurs at the benzimidazole group for each model resulting in free non-H-bonded and tag-bound OH stretches highest in energy (red). The weakly H-bonded $N_{(3)}H^+$ stretches are identified in blue. The $N_{(1)}H^+$ stretches are identified in green. Models (**5**) and (**6**) display signatures of relatively strong H-bonding between the benzimidazole NH^+ and the backbone Tyr ethyl ester carbonyl.

shows a pair of transitions at 3597 and 3641 cm^{-1} corresponding to tagged and untagged OH isomers, respectively. The much weaker untagged OH stretch indicates that the tag predominantly attaches to the OH group. The H-bonded $N_{(3)}H^+$ stretch occurs at 3444 cm^{-1} with a red-shifted shoulder either due to a tag isomer or one of the weaker amine NH_2 stretches. A new, broad feature appears near 3280 cm^{-1} (green) that is attributed to a H-bond between the $N_{(1)}H^+$ and the tyrosine ethyl ester carbonyl group. The assignments are consistent with the harmonic spectrum predicted for the lowest-energy structure found (Figure S5).

Compound (**6**) is the same tyrosine derivative of (**1**) with methylated benzimidazole appended at the *ortho* position. Despite the addition of a bulky methyl group at the $N_{(1)}$ position, a non-H-bonded phenolic OH stretch is still observed near 3600 cm^{-1}. This suggests again that benzimidazole (this time the $N_{(3)}$ position) is the favored protonation site. The lack of a broad H-bonded amide NH^+ stretch near 2500 cm^{-1}, as was observed in (**1**), indicates that benzimidazole protonation is the only constitutional isomer present. Two conformers are possible: one where $N_{(3)}H^+$ forms a H-bond to the phenolic oxygen or one where $N_{(3)}H^+$ forms a H-bond with the ethyl ester carbonyl. The spectrum and calculations (Figure S6) are consistent with the latter being the dominant conformer, although we cannot rule out the presence of the former. The transition near 3410 cm^{-1} is, therefore, assigned to the backbone amide NH stretch. The significant intensity gain and breadth of the CH stretch region (green) is assigned to a

https://doi.org/10.1021/acs.jpca.1c05879
J. Phys. Chem. A 2021, 125, 9288−9297

relatively strong H-bond between the benzimidazole $N_{(3)}H^+$ and ethyl ester carbonyl groups. The complexity of CH stretch regions likely manifests from the presence of strong anharmonic coupling and intensity sharing between the H-bonded $N_{(3)}H^+$ stretch, background doorway states, and CH stretches.[34,43]

DISCUSSION

Phenol-Benzimidazole OH−$N_{(3)}$ H-Bond in (3). The most important feature observed is the significantly red-shifted and broadened OH stretch in compound (**3**). The phenol-benzimidazole scaffold results in a cyclic intramolecular H-bond (CIHB), a class of systems that has been well studied under jet-cooled or cryogenic trapping conditions. H-bonded OH or NH stretch transitions in these systems are likewise typically broad (usually several hundred wavenumbers) and often display rich substructure. The breadths of the shared proton transitions are often attributed to one of two main sources: (1) anharmonic coupling of the OH/NH stretch to dark background "doorway" states, particularly overtones and combination bands involving OH/NH bending modes in Fermi-resonance-type interactions. (2) High sensitivity of the strongly H-bonded OH/NH stretch frequency to structural variations accessible through zero-point heavy-atom displacements. It is instructive, therefore, to examine the phenol-benzimidazole H-bond in (**3**) in the context of several recently studied systems containing strong CIHB's.

Starting with neutral systems, Zwier and Sibert have investigated the curious case of methyl anthranilate (methyl 2-aminobenzoate).[44] In the ground electronic state, one of the amine NH_2 protons forms a very weak H-bond with the neighboring carbonyl of the methyl carboxylate group. The NH_2 stretch vibrations retain the symmetric and antisymmetric character, and the vibrational spectrum is well reproduced at the harmonic level. In the excited S_1 state, however, a much stronger H-bond is expected due to a significant shift in electron density between NH_2 and carbonyl groups. A single non-H-bonded free NH was observed at higher frequencies, but the H-bonded NH stretch, predicted to appear near 2900 cm^{-1}, was completely absent. Theoretical modeling pointed to an extreme case of anharmonic coupling between the shared proton stretch and NH bending modes that dilute the proton stretch intensity among background doorway states that span about a thousand wavenumbers. This is closely related to the ~500 cm^{-1} broad, but highly substructured, OH stretch region observed in gaseous carboxylic acid dimers.[45−47] The substructure pattern can be nearly quantitatively attributed to Fermi-resonance-type interactions between OH stretches and background states involving OH bending modes.[48]

Johnson and McCoy have made great progress in unraveling the breadth of OH/NH stretches in CIHB systems involving ionic H-bonds. In the case of protonated 1,8-disubstituted naphthalene derivatives, a complicated substructure pattern was observed near 3000 cm^{-1} attributed to a strong H-bond between the NH^+ group at the 1-position with a H-bond acceptor group at the 8-position.[43] Selective exchange of NH^+ to ND^+ yielded a much simpler ND^+ stretch pattern with only a few sharp transitions and, critically, revealed the NH^+ bend to have significant contributions to numerous fingerprint transitions. This leads to a multitude of dark background overtone and combination bands containing NH^+ bend character that can mix with the NH^+ stretch in a similar scenario to excited methyl anthranilate. A Fermi-resonance model that took into account cubic coupling between the zeroth-order NH^+ stretch bright state and dark doorway states quite accurately reproduced the observed spectral pattern. This same model was later used to explain the origin of the breadth of the H-bonded NH^+ and ND^+ stretches in $GlyGlyH^+/D^+$.[34]

Using the same Fermi-resonance model, we predict the degree of anharmonic mixing between the OH stretch and doorway states using cubic coupling constants computed from an anharmonic VPT2 calculation on a smaller, computationally tractable phenol-benzimidazole neutral dyad complex (Figure 4). Although not the same system, we extract useful

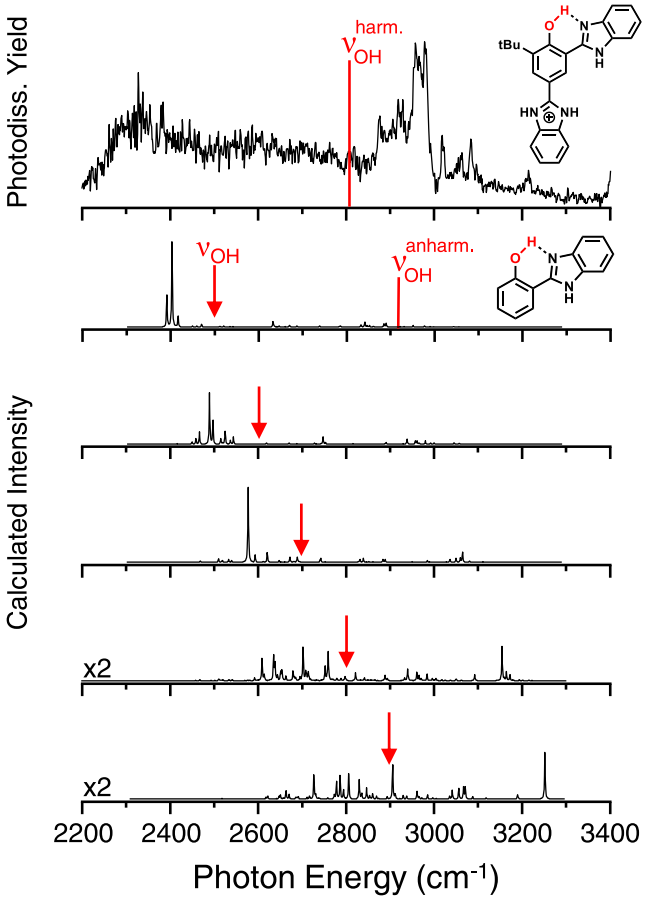

Figure 4. Comparison of the experimental OH stretch feature in compound (**3**) to anharmonic predictions for a simpler phenol-benzimidazole model that takes into account cubic coupling between the OH stretch and doorway states involving overtones and combination bands of the OH bend and O−N soft modes. The computed unscaled harmonic OH stretch frequency is indicated in the top trace for compound (**3**). The anharmonic VPT2 OH stretch frequency for the smaller model is indicated in the second trace. Red arrows indicate the zeroth-order frequency of the OH stretch used in the anharmonic analysis. The bottom two traces are multiplied by 2 for better visualization.

information about the nature of the coupling between the H-bonded OH stretch, OH bends, and O−N soft modes. Importantly, harmonic calculations predict similar behavior in the critical OH bend region for both systems (Figure S7). In particular, the harmonic calculations for both species demonstrate that fingerprint transitions spanning 1200−1700 cm^{-1} cannot be easily defined in terms of local mode vibrations and are instead best described as admixtures of OH bend, NH

https://doi.org/10.1021/acs.jpca.1c05879
J. Phys. Chem. A 2021, 125, 9288−9297

bends, CH bends, and C=C stretches. About a dozen modes between 1200 and 1650 cm^{-1} are predicted to have significant OH bend character in (**3**) and the smaller model, with the strongest transitions occurring in the 1500−1650 cm^{-1} range. Modest matrix elements on the order of 1−25 cm^{-1} are predicted between the OH stretch and overtones/combination bands involving these OH bending modes for the smaller dyad. Interestingly, the largest cubic coupling terms arise from coupling between the OH stretch and three OH stretch + O−N soft mode combination bands, with matrix elements of ∼80 cm^{-1}. Diagonalization of a matrix containing the OH stretch and ∼500 doorway states yields the spectra shown in Figure 4 for several zeroth-order OH stretch frequencies (assuming all initial intensity originates from the OH stretch bright state). This procedure indeed predicts significant anharmonic mixing and dilution of the OH stretch intensity, particularly when the OH stretch originates between ∼2800 and 3100 cm^{-1}. This is to be expected given the predicted frequencies of the strongest OH bending modes, which will place the greatest density of doorway states in this region. No single spectrum, however, captures the full breadth of the observed band. OH stretches set to lower frequencies result in much simplified band patterns due to the lower density of states involving OH bends and smaller matrix elements. Compound (**3**) will certainly have a higher density of OH bend doorway states throughout the entire spectral region, and we would anticipate larger matrix elements as the H-bond in (**3**) is predicted to be much stronger than that in the simpler model. Nevertheless, the similarity of the predicted OH bending region in both systems suggests that anharmonic mixing will still be strongest at frequencies >2700 cm^{-1} in (**3**), and it seems unlikely that anharmonic mixing of the OH stretch at a single frequency would account for the entire breadth of the observed transition.

A second possible contribution to the OH stretch breadth would be a high sensitivity of the OH vibrational frequency to structural variations along the proton-transfer coordinate through heavy-atom displacements accessible at the zero-point level. Perhaps the most extreme example of this phenomenon was reported in $M^{2+}OH^{-}(H_2O)_n$ (M = Ca, Mg) clusters by Johnson et al.,[33] where the OH stretch of a first shell water molecule H-bonded to the hydroxide ion was observed to span >1000 cm^{-1}. The breadth was quantitatively reproduced using a model that sampled geometries accessible at 0 K from zero-point heavy-atom displacements and adiabatically separated the high-frequency OH stretch from the low-frequency soft modes. Strong correlations were predicted between the OH stretch frequency and the O−O distance and OH−O water-hydroxide bend angle. This model was later used to rationalize the broad CIHB proton stretch observed in the singly protonated oxalate anion, $HO_2CCO_2^-$, which spans ∼2500−3200 cm^{-1}.[32] In that scenario, the OH stretch was found to be highly correlated with the COH angle but, interestingly, uncorrelated with the O−O distance. This procedure also accurately accounted for the narrower (∼400 cm^{-1}) breadth of the OD stretch in the deuterated oxalate isotopologue.

While the very strong H-bond in (**3**) would suggest that the OH stretch frequency will likely be quite sensitive to heavy-atom displacements that perturb the proton-transfer coordinate, the rigidity of the phenol-benzimidazole scaffold likely limits the distribution of O−N distances within the ensemble compared to the more flexible oxalate and cluster systems. The large cubic coupling constants predicted between the O−N soft modes and the OH stretch, however, suggests even minimal displacements in d_{ON} could have a strong influence on the OH stretch frequency. As in the case of oxalate, the OH stretch might also be highly sensitive to displacements in the COH angle. We do not, however, attempt to quantify the effects of zero-point displacements here.

It seems most plausible that the OH stretch breadth originates from a complex interplay between heavy-atom displacements that vary the OH stretch frequency and anharmonic Fermi-resonance-type coupling to doorway states. As evidenced in Figure 4, a modest shift of the OH stretch frequency drastically changes the degree of mixing with the doorway states. Collectively, the computed anharmonic spectra in Figure 4 can be used to rationalize the breadth of the OH stretch. Configurations that lead to highly red-shifted OH stretch frequencies (2300−2600 cm^{-1}) result in less anharmonic mixing due to a lower density of doorway states involving the OH bend. This results in intensity sharing between fewer modes, yielding the relatively sharp and intense onset of the OH stretch near 2300 cm^{-1}. Configurations with OH stretch frequencies in the 2800−3000 cm^{-1} range mix more strongly with a higher density of doorway states leading to broader but weaker spectral patterns.

These interpretations are corroborated by Van Hoozen and Petersen, who analyzed the broad solution-phase OH stretching transitions observed in a series of carboxylic acid/nitrogen-containing aromatic base H-bonded dimers.[49−52] These model dimers display complicated OH stretching transitions with multiple broad humps spanning ∼1000 cm^{-1} in solution. The computational models developed by Van Hoozen and Petersen took into account Fermi-resonance coupling between the OH stretch and OH bending modes and coupling to low-frequency H-bond stretching motion between the monomers. The calculations showed that the hump substructure can be attributed to the OH stretch-bend Fermi-resonance interactions modes, while the overall breadth originates from low-frequency motions that modulate H-bond distances and thus the frequency of the OH stretch. The calculations also predicted the OH stretch to have an intrinsic (0 K) line width of >200 cm^{-1} due to the distribution of H-bond distances between monomers at the zero-point level.[49] Critically, these computational models demonstrated that the OH stretch frequency modulation induced by low-frequency H-bond stretching motions also strongly modulates the OH stretch-bend Fermi-resonance coupling.[50]

To help verify these conclusions, we recorded the spectrum of the isotopologue with the four labile protons substituted with deuterons (d_4-(**3**)). Figure 5b,c shows the 1200−2100 cm^{-1} region for the all-H and d_4 isotopologue species, respectively. The corresponding harmonic predictions (scaled by 0.99) are given in Figure 5a,d, respectively. The changes observed in the fingerprint region are quite complicated, with almost every transition shifting to some degree. This observation demonstrates the highly mixed nature of normal modes and the significant NH/OH bending contributions to most fingerprint transitions (Figure S7). In stark contrast, the predicted normal modes in this region for the deuterated isotopologue have no OD bend character (Figure S8). Instead, a single localized OD bend mode is predicted near 1100 cm^{-1}. A broad feature spanning ∼1700−2000 cm^{-1} is observed in the spectrum of d_4-(**3**) that must arise from the H-bonded phenolic OD stretch (Figure 5c, red). While much narrower

https://doi.org/10.1021/acs.jpca.1c05879
J. Phys. Chem. A 2021, 125, 9288−9297

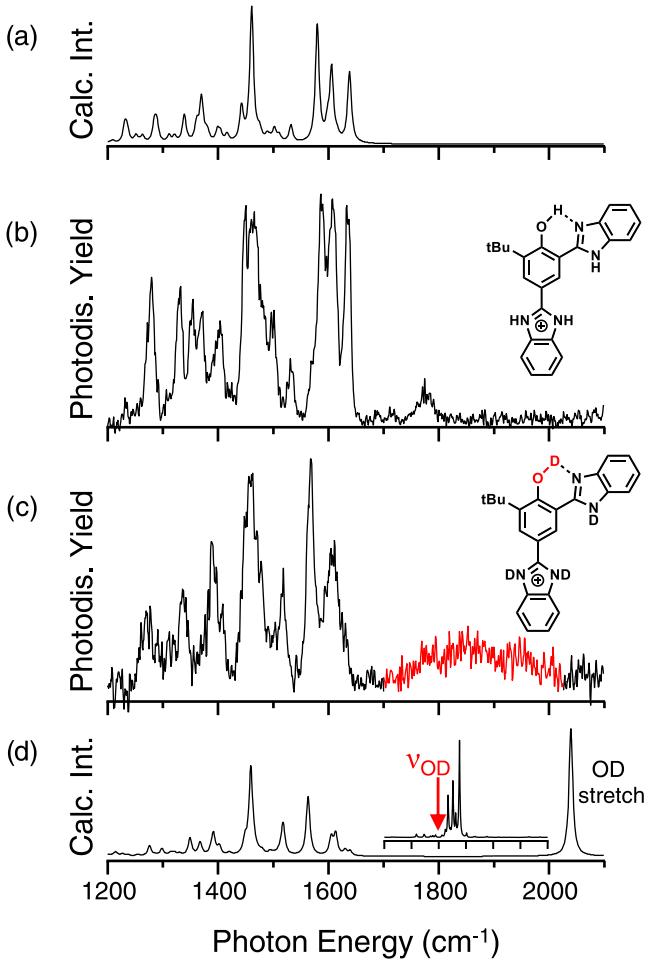

Figure 5. (a, b) Harmonic and experimental vibrational spectra of compound (**3**) in the 1200−2100 cm^{-1} region, respectively. (c, d) Harmonic and experimental spectra of the d_4-(**3**) isotopologue, respectively. The OD stretch (red) is assigned to the broad transition centered near 1850 cm^{-1}. The lower-frequency normal modes are predicted to be complicated admixtures of OH bend, NH bends, CH bends, and C═C stretches in all-H (**3**) but more localized in d_4-(**3**). Supporting Information Figures S7 and S8 show normal mode displacement vectors for the most intense transitions. Inset (d): Anharmonic Fermi-resonance analysis for the smaller deuterated phenol-benzimidazole dyad for an OD stretch bright state frequency of 1800 cm^{-1}.

than the OH stretch, the OD stretch does not simplify to a set of sharper transitions as was observed in $GlyGlyD^+$ or the deuterated 1,8-disubstituted naphthalene ions.[32,43] Instead, the broad OD stretch is more reminiscent of single-hump OD stretches observed in the solution-phase H-bonded dimer models analyzed by Van Hoozen and Petersen.[50] Fermi-resonance analysis on the smaller deuterated phenol-benzimidazole model (Figure 5d inset, zeroth-order OD stretch set to 1800 cm^{-1}) predicts a narrow band pattern as anticipated due to the more localized OD bend. Analyses for different OD stretch zeroth-order frequencies yield similar results (Figure S9). While Fermi-resonance interactions certainly contribute, the overall breadth of the OD stretch seems most consistent with a distribution of OD stretching frequencies arising from structural perturbations along the proton-transfer coordinate present at the zero-point level.

Hydrogen-Bonding Motifs in Compounds (4)−(6). The appearance of free OH stretches in (**4**)−(**6**) is consistent with protonation at the benzimidazole $N_{(3)}$ position despite the presence of much more basic amine/amide groups (pK_b ∼8 for benzimidazole vs ∼3−4 for amines; the increased conjugation in the dyads should make the $N_{(3)}$ location even less basic). NMR spectra for the neutral synthesized compounds show highly downshifted (∼12 ppm) hydroxyl peaks as anticipated for strong OH−$N_{(3)}$ H-bonds and are consistent with previous reports. It appears, then, that isomerization of the protonation site is occurring during the ionization/ion transfer process. This phenomenon has been observed previously and has been an important topic in terms of mass spectrometric analyses as the preferred protonation site can differ between the solution and gas phase.[53−55] Our calculations do, in fact, predict that structures with benzimidazole protonated are much lower in energy compared to amine/amide protonation for isolated gas-phase ions (Supporting Information). While the exact mechanism of this process is unknown, the hydroxyl NMR peaks are quite broad indicating facile exchange of the proton with solvent and suggesting that the OH−$N_{(3)}$ motif is somewhat floppy and susceptible to this isomerization process. It is clear that future studies will likely require appending the model scaffold to a charged metal species such as $Ru(bpy)_3^{2+}$ to avoid this undesirable protonation isomer or optimizing source conditions for softer generation and transfer of ions that kinetically trap the solution-phase isomer.

It is also curious that compound (**4**), which is identical to (**3**) except for substitution of *para* benzimidazole for ethyl amine, only shows protonation at *ortho* benzimidazole and does not form an isomer with the same strong OH−$N_{(3)}$ H-bond seen in (**3**). Calculations predict the HO−$H^+N_{(3)}$ isomer to be much higher in energy in (**3**), while this isomer is actually much lower in energy for (**4**), even with the steric hindrance of the bulky *tert*-butyl group. The computed structure of the higher-energy OH−$N_{(3)}$ isomer of (**4**) gives only a marginally longer d_{ON} of 2.55 Å, yet it predicts a 100 cm^{-1} blue shift of the OH stretch compared to that predicted for (**3**) (Figure S10). Further, the simplified dyad used in anharmonic VPT2 calculations discussed above predicts a much weaker OH−$N_{(3)}$ H-bond compared to (**3**). In fact, the anharmonic OH stretch in the simplified dyad is over 100 cm^{-1} blue-shifted compared to the unscaled harmonic OH stretch predicted for (**3**). Collectively, these observations suggest that the enhanced electron conjugation present in (**3**), due to the added *para* benzimidazole group, are quite significant and act to strengthen and stabilize the OH−$N_{(3)}$ H-bond in that compound. The influence of conjugation effects on measured PCET kinetics within dyad models has been raised previously,[8,9,17] and our initial results indicate that they indeed strongly affect the OH−$N_{(3)}$ H-bond interaction.

Compound (**5**) contains an additional H-bond interaction between $N_{(1)}H^+$ and ethyl ester carbonyl not present in the other compounds. This H-bond appears much stronger than the HO−$^+HN_{(3)}$ interaction, as evidenced by the highly red-shifted and broadened $N_{(1)}H^+$ stretch (green feature, Figure 3c) and consistent with harmonic predictions (Figure S5). The presence of the $N_{(1)}H^+$−carbonyl H-bond results in a computed dihedral twist between the phenol and benzimidazole rings of about 20° away from planarity. This twist acts to weaken the HO−$^+HN_{(3)}$ H-bond resulting in the observed ∼40 cm^{-1} blue shift of the $N_{(3)}H^+$ stretch compared to that in

https://doi.org/10.1021/acs.jpca.1c05879
J. Phys. Chem. A 2021, 125, 9288−9297

compound (**2**), where the additional H-bond is absent. Even more interesting is that a $N_{(3)}H^+$−carbonyl H-bond is still preferred over a HO−$^+HN_{(3)}$ H-bond in (**6**), where the bulky methyl group substituted at the $N_{(1)}$ position should cause a significant steric hindrance when pointed toward the OH. Indeed, the dihedral twist is computed to be about 50° away from planarity in (**6**), which will act to break the resonance stabilization of the ring system. This larger dihedral twist allows for the formation of a stronger $N_{(3)}H^+$−carbonyl H-bond compared to that in (**5**). This raises an important question regarding the influence of secondary H-bonding interactions of the $N_{(1)}H$ group (both in models and biological Tyr−His systems) on the OH−$N_{(3)}$ H-bond and PCET dynamics. Unfortunately, the unintended protonation of the benzimidazole group does not allow us to fully assess this effect at this time, but will be an important target in future studies.

SUMMARY

Cryogenic ion vibrational spectra of a series of phenol-benzimidazole PCET model compounds have been recorded in the OH/NH stretch region. One of these compounds, model (**3**), displays a highly red-shifted and broadened phenol OH stretch consistent with a very strong H-bonding interaction with the $N_{(3)}$ atom on benzimidazole. The breadth is attributed to anharmonic coupling with background doorway states with OH bend and O−N soft mode character and to heavy-atom displacements that modulate the OH stretch frequency and, consequently, the coupling between states. Further CIVS studies are clearly warranted to establish how the OH−$N_{(3)}$ H-bond and ground-state proton-transfer potential energy surface evolve with O−N distance, temperature (excitation of proton-transfer soft modes), secondary H-bonding interactions, elimination of resonance stabilization, and solvent interactions. While more robust theoretical calculations are needed to disentangle the microscopic mechanics that contribute to the red shift and breadth of the phenolic OH stretch, our results provide an initial experimental benchmark with which to model the electronic ground-state proton-transfer potential energy surface, anharmonic coupling to dark doorway states, and coupling to the key proton-transfer coordinates within PCET model systems.

ASSOCIATED CONTENT

Supporting Information

The Supporting Information is available free of charge at https://pubs.acs.org/doi/10.1021/acs.jpca.1c05879.

Synthetic protocols and NMR characterization of model compounds; computed structures and harmonic vibrational spectra of compounds (**1**)−(**6**) (Figures S1−S6); comparison of the computed harmonic spectra and normal mode displacements in the 1200−1700 cm^{-1} region for model (**3**) and the smaller phenol-benzimidazole dyad used for anharmonic calculations (Figure S7); comparison of computed harmonic spectra and normal mode displacements of the deuterated isotopologues of (**3**) and the smaller phenol-benzimidazole dyad (Figure S8); Fermi-resonance results for the deuterated phenol-benzimidazole dyad with varying OD stretch zeroth-order frequencies (Figure S9); and comparison of the computed structures and harmonic spectra of (**3**) and the OH−$N_{(3)}$ isomer of (**4**) (Figure S10) (PDF)

AUTHOR INFORMATION

Corresponding Author

Joseph A. Fournier − *Department of Chemistry, Washington University in St. Louis, St. Louis, Missouri 63130, United States*; orcid.org/0000-0001-7569-9176; Email: jfournier@wustl.edu

Author

Liangyi Chen − *Department of Chemistry, Washington University in St. Louis, St. Louis, Missouri 63130, United States*

Complete contact information is available at: https://pubs.acs.org/10.1021/acs.jpca.1c05879

Notes

The authors declare no competing financial interest.

ACKNOWLEDGMENTS

The authors gratefully acknowledge the National Science Foundation for support through a CAREER Award (grant number CHE-2044927) and Washington University in St. Louis and the Department of Chemistry for generous start-up funding. The authors thank Prof. Tim Wencewicz and his group for helpful discussions and assistance in synthesizing the model compounds.

REFERENCES

(1) Weinberg, D. R.; Gagliardi, C. J.; Hull, J. F.; Murphy, C. F.; Kent, C. A.; Westlake, B. C.; Paul, A.; Ess, D. H.; McCafferty, D. G.; Meyer, T. J. Proton-Coupled Electron Transfer. *Chem. Rev.* **2012**, *112*, 4016−4093.

(2) Darcy, J. W.; Koronkiewicz, B.; Parada, G. A.; Mayer, J. M. A Continuum of Proton-Coupled Electron Transfer Reactivity. *Acc. Chem. Res.* **2018**, *51*, 2391−2399.

(3) Migliore, A.; Polizzi, N. F.; Therien, M. J.; Beratan, D. N. Biochemistry and Theory of Proton-Coupled Electron Transfer. *Chem. Rev.* **2014**, *114*, 3381−3465.

(4) Reece, S. Y.; Nocera, D. G. Proton-Coupled Electron Transfer in Biology: Results from Synergistic Studies in Natural and Model Systems. *Annu. Rev. Biochem.* **2009**, *78*, 673−699.

(5) Umena, Y.; Kawakami, K.; Shen, J. R.; Kamiya, N. Crystal Structure of Oxygen-Evolving Photosystem II at a Resolution of 1.9 Å. *Nature* **2011**, *473*, 55−60.

(6) Markle, T. F.; Rhile, I. J.; DiPasquale, A. G.; Mayer, J. M. Probing Concerted Proton-Electron Transfer in Phenol-Imidazoles. *Proc. Natl. Acad. Sci. U.S.A.* **2008**, *105*, 8185−8190.

(7) Irebo, T.; Reece, S. Y.; Sjodin, M.; Nocera, D. G.; Hammarstrom, L. Proton-Coupled Electron Transfer of Tyrosine Oxidation: Buffer Dependence and Parallel Mechanisms. *J. Am. Chem. Soc.* **2007**, *129*, 15462−15464.

(8) Zhang, M. T.; Irebo, T.; Johansson, O.; Hammarstrom, L. Proton-Coupled Electron Transfer from Tyrosine: A Strong Rate Dependence on Intramolecular Proton Transfer Distance. *J. Am. Chem. Soc.* **2011**, *133*, 13224−13227.

(9) Markle, T. F.; Zhang, M. T.; Santoni, M. P.; Johannissen, L. O.; Hammarstrom, L. Proton-Coupled Electron Transfer in a Series of Ruthenium-Linked Tyrosines with Internal Bases: Evaluation of a Tunneling Model for Experimental Temperature-Dependent Kinetics. *J. Phys. Chem. B* **2016**, *120*, 9308−9321.

(10) Bowring, M. A.; Bradshaw, L. R.; Parada, G. A.; Pollock, T. P.; Fernandez-Teran, R. J.; Kolmar, S. S.; Mercado, B. Q.; Schlenker, C. W.; Gamelin, D. R.; Mayer, J. M. Activationless Multiple-Site Concerted Proton-Electron Tunneling. *J. Am. Chem. Soc.* **2018**, *140*, 7449−7452.

(11) Huynh, M. T.; Mora, S. J.; Villalba, M.; Tejeda-Ferrari, M. E.; Liddell, P. A.; Cherry, B. R.; Teillout, A. L.; Machan, C. W.; Kubiak,

C. P.; Gust, D.; et al. Concerted One-Electron Two-Proton Transfer Processes in Models Inspired by the Tyr-His Couple of Photosystem II. *ACS Cent. Sci.* **2017**, *3*, 372−380.
(12) Manbeck, G. F.; Fujita, E.; Concepcion, J. J. Proton-Coupled Electron Transfer in a Strongly Coupled Photosystem II-Inspired Chromophore-Imidazole-Phenol Complex: Stepwise Oxidation and Concerted Reduction. *J. Am. Chem. Soc.* **2016**, *138*, 11536−11549.
(13) Lennox, J. C.; Dempsey, J. L. Influence of Proton Acceptors on the Proton-Coupled Electron Transfer Reaction Kinetics of a Ruthenium-Tyrosine Complex. *J. Phys. Chem. B* **2017**, *121*, 10530−10542.
(14) Pagba, C. V.; McCaslin, T. G.; Chi, S. H.; Perry, J. W.; Barry, B. A. Proton-Coupled Electron Transfer and a Tyrosine-Histidine Pair in a Photosystem II-Inspired β-Hairpin Maquette: Kinetics on the Picosecond Time Scale. *J. Phys. Chem. B* **2016**, *120*, 1259−1272.
(15) Pannwitz, A.; Wenger, O. S. Photoinduced Electron Transfer Coupled to Donor Deprotonation and Acceptor Protonation in a Molecular Triad Mimicking Photosystem II. *J. Am. Chem. Soc.* **2017**, *139*, 13308−13311.
(16) Yoneda, Y.; Mora, S. J.; Shee, J.; Wadsworth, B. L.; Arsenault, E. A.; Hait, D.; Kodis, G.; Gust, D.; Moore, G. F.; Moore, A. L.; et al. Electron-Nuclear Dynamics Accompanying Proton-Coupled Electron Transfer. *J. Am. Chem. Soc.* **2021**, *143*, 3104−3112.
(17) Glover, S. D.; Parada, G. A.; Markle, T. F.; Ott, S.; Hammarstrom, L. Isolating the Effects of the Proton Tunneling Distance on Proton-Coupled Electron Transfer in a Series of Homologous Tyrosine-Base Model Compounds. *J. Am. Chem. Soc.* **2017**, *139*, 2090−2101.
(18) Johannissen, L. O.; Irebo, T.; Sjodin, M.; Johansson, O.; Hammarstrom, L. The Kinetic Effect of Internal Hydrogen Bonds on Proton-Coupled Electron Transfer from Phenols: A Theoretical Analysis with Modeling of Experimental Data. *J. Phys. Chem. B* **2009**, *113*, 16214−16225.
(19) Knapp, M. J.; Rickert, K.; Klinman, J. P. Temperature-Dependent Isotope Effects in Soybean Lipoxygenase-1: Correlating Hydrogen Tunneling with Protein Dynamics. *J. Am. Chem. Soc.* **2002**, *124*, 3865−3874.
(20) Hay, S.; Scrutton, N. S. Good Vibrations in Enzyme-Catalysed Reactions. *Nat. Chem.* **2012**, *4*, 161−168.
(21) Layfield, J. P.; Hammes-Schiffer, S. Hydrogen Tunneling in Enzymes and Biomimetic Models. *Chem. Rev.* **2014**, *114*, 3466−3494.
(22) Megiatto, J. D., Jr.; Mendez-Hernandez, D. D.; Tejeda-Ferrari, M. E.; Teillout, A. L.; Llansola-Portoles, M. J.; Kodis, G.; Poluektov, O. G.; Rajh, T.; Mujica, V.; Groy, T. L.; et al. A Bioinspired Redox Relay That Mimics Radical Interactions of the Tyr-His Pairs of Photosystem II. *Nat. Chem.* **2014**, *6*, 423−428.
(23) Hammes-Schiffer, S.; Soudackov, A. V. Proton-Coupled Electron Transfer in Solution, Proteins, and Electrochemistry. *J. Phys. Chem. B* **2008**, *112*, 14108−14123.
(24) Hammes-Schiffer, S. Theoretical Perspectives on Proton-Coupled Electron Transfer Reactions. *Acc. Chem. Res.* **2001**, *34*, 273−281.
(25) Sarkar, S.; Maitra, A.; Lake, W. R.; Warburton, R. E.; Hammes-Schiffer, S.; Dawlaty, J. M. Mechanistic Insights About Electrochemical Proton-Coupled Electron Transfer Derived from a Vibrational Probe. *J. Am. Chem. Soc.* **2021**, *143*, 8381−8390.
(26) Wolk, A. B.; Leavitt, C. M.; Garand, E.; Johnson, M. A. Cryogenic Ion Chemistry and Spectroscopy. *Acc. Chem. Res.* **2014**, *47*, 202−210.
(27) Garand, E. Spectroscopy of Reactive Complexes and Solvated Clusters: A Bottom-up Approach Using Cryogenic Ion Traps. *J. Phys. Chem. A* **2018**, *122*, 6479−6490.
(28) Heine, N.; Asmis, K. R. Cryogenic Ion Trap Vibrational Spectroscopy of Hydrogen-Bonded Clusters Relevant to Atmospheric Chemistry. *Int. Rev. Phys. Chem.* **2015**, *34*, 1−34.
(29) Yang, N.; Edington, S. C.; Choi, T. H.; Henderson, E. V.; Heindel, J. P.; Xantheas, S. S.; Jordan, K. D.; Johnson, M. A. Mapping the Temperature-Dependent and Network Site-Specific Onset of Spectral Diffusion at the Surface of a Water Cluster Cage. *Proc. Natl. Acad. Sci. U.S.A.* **2020**, *117*, 26047−26052.
(30) Duong, C. H.; Gorlova, O.; Yang, N.; Kelleher, P. J.; Johnson, M. A.; McCoy, A. B.; Yu, Q.; Bowman, J. M. Disentangling the Complex Vibrational Spectrum of the Protonated Water Trimer, $H^+(H_2O)_3$, with Two-Color IR-IR Photodissociation of the Bare Ion and Anharmonic VSCF/VCI Theory. *J. Phys. Chem. Lett.* **2017**, *8*, 3782−3789.
(31) Fagiani, M. R.; Knorke, H.; Esser, T. K.; Heine, N.; Wolke, C. T.; Gewinner, S.; Schöllkopf, W.; Gaigeot, M.-P.; Spezia, R.; Johnson, M. A.; et al. Gas Phase Vibrational Spectroscopy of the Protonated Water Pentamer: The Role of Isomers and Nuclear Quantum Effects. *Phys. Chem. Chem. Phys.* **2016**, *18*, 26743−26754.
(32) Wolke, C. T.; DeBlase, A. F.; Leavitt, C. M.; McCoy, A. B.; Johnson, M. A. Diffuse Vibrational Signature of a Single Proton Embedded in the Oxalate Scaffold, $HO_2CCO_2^-$. *J. Phys. Chem. A* **2015**, *119*, 13018−13024.
(33) Johnson, C. J.; Dzugan, L. C.; Wolk, A. B.; Leavitt, C. M.; Fournier, J. A.; McCoy, A. B.; Johnson, M. A. Microhydration of Contact Ion Pairs in $M^{2+}OH^-(H_2O)_{n=1-5}$ (M = Mg, Ca) Clusters: Spectral Manifestations of a Mobile Proton Defect in the First Hydration Shell. *J. Phys. Chem. A* **2014**, *118*, 7590−7597.
(34) Leavitt, C. M.; Deblase, A. F.; Johnson, C. J.; Van Stipdonk, M.; McCoy, A. B.; Johnson, M. A. Hiding in Plain Sight: Unmasking the Diffuse Spectral Signatures of the Protonated N-Terminus in Isolated Dipeptides Cooled in a Cryogenic Ion Trap. *J. Phys. Chem. Lett.* **2013**, *4*, 3450−3457.
(35) Fournier, J. A.; Carpenter, W. B.; Lewis, N. H. C.; Tokmakoff, A. Broadband 2D IR Spectroscopy Reveals Dominant Asymmetric $H_5O_2^+$ Proton Hydration Structures in Acid Solutions. *Nat. Chem.* **2018**, *10*, 932−937.
(36) Thämer, M.; De Marco, L.; Ramasesha, K.; Mandal, A.; Tokmakoff, A. Ultrafast 2D IR Spectroscopy of the Excess Proton in Liquid Water. *Science* **2015**, *350*, 78−82.
(37) Dahms, F.; Fingerhut, B. P.; Nibbering, E. T. J.; Pines, E.; Elsaesser, T. Large-Amplitude Transfer Motion of Hydrated Excess Protons Mapped by Ultrafast 2D IR Spectroscopy. *Science* **2017**, *357*, 491−495.
(38) Stingel, A. M.; Petersen, P. B. Couplings across the Vibrational Spectrum Caused by Strong Hydrogen Bonds: A Continuum 2D IR Study of the 7-Azaindole-Acetic Acid Heterodimer. *J. Phys. Chem. B* **2016**, *120*, 10768−10779.
(39) Kamrath, M. Z.; Relph, R. A.; Guasco, T. L.; Leavitt, C. M.; Johnson, M. A. Vibrational Predissociation Spectroscopy of the H_2-Tagged Mono- and Dicarboxylate Anions of Dodecanedioic Acid. *Int. J. Mass Spectrom.* **2011**, *300*, 91−98.
(40) Marsh, B. M.; Zhou, J.; Garand, E. Vibrational Spectroscopy of Small Hydrated $CuOH^+$ Clusters. *J. Phys. Chem. A* **2014**, *118*, 2063−2071.
(41) Frisch, M. J.; Trucks, G. W.; Schlegel, H. B.; Scuseria, G. E.; Robb, M. A.; Cheeseman, J. R.; Scalmani, G.; Barone, V.; Mennucci, B.; Petersson, G. A. et al. *Gaussian 09*; Gaussian, Inc.: Wallingford, CT, 2009.
(42) Klots, T. D.; Devlin, P.; Collier, W. B. Heteroatom Derivatives of Indene V. Vibrational Spectra of Benzimidazole. *Spectrochim. Acta, Part A* **1997**, *53*, 2445−2456.
(43) DeBlase, A. F.; Bloom, S.; Lectka, T.; Jordan, K. D.; McCoy, A. B.; Johnson, M. A. Origin of the Diffuse Vibrational Signature of a Cyclic Intramolecular Proton Bond: Anharmonic Analysis of Protonated 1,8-Disubstituted Naphthalene Ions. *J. Chem. Phys.* **2013**, *139*, No. 024301.
(44) Blodgett, K. N.; Fischer, J. L.; Zwier, T. S.; Sibert, E. L. The Missing NH Stretch Fundamental in S_1 Methyl Anthranilate: IR-UV Double Resonance Experiments and Local Mode Theory. *Phys. Chem. Chem. Phys.* **2020**, *22*, 14077−14087.
(45) Ito, F. Infrared Spectra of $(HCOOH)_2$ and $(DCOOH)_2$ in Rare Gas Matrices: A Comparative Study with Gas Phase Spectra. *J. Chem. Phys.* **2008**, *128*, No. 114310.

https://doi.org/10.1021/acs.jpca.1c05879
J. Phys. Chem. A 2021, 125, 9288−9297

(46) Häber, T.; Schmitt, U.; Emmeluth, C.; Suhm, M. A. Ragout-Jet FTIR Spectroscopy of Cluster Isomerism and Cluster Dynamics: From Carboxylic Acid Dimers to N_2O Nanoparticles. *Faraday Discuss.* **2001**, *118*, 331−359.
(47) Florio, G. M.; Sibert, E. L.; Zwier, T. S. Fluorescence-Dip IR Spectra of Jet-Cooled Benzoic Acid Dimer in its Ground and First Excited Singlet States. *Faraday Discuss.* **2001**, *118*, 315−330.
(48) Florio, G. M.; Zwier, T. S.; Myshakin, E. M.; Jordan, K. D.; Sibert, E. L. Theoretical Modeling of the OH Stretch Infrared Spectrum of Carboxylic Acid Dimers Based on First-Principles Anharmonic Couplings. *J. Chem. Phys.* **2003**, *118*, 1735−1746.
(49) Van Hoozen, B. L.; Petersen, P. B. Origin of the 900 cm^{-1} Broad Double-Hump OH Vibrational Feature of Strongly Hydrogen-Bonded Carboxylic Acids. *J. Chem. Phys.* **2015**, *142*, No. 104308.
(50) Van Hoozen, B. L.; Petersen, P. B. Origin of the Hadzi ABC Structure: An Ab Initio Study. *J. Chem. Phys.* **2015**, *143*, No. 184305.
(51) Van Hoozen, B. L.; Petersen, P. B. Vibrational Tug-of-War: The pK_a Dependence of the Broad Vibrational Features of Strongly Hydrogen-Bonded Carboxylic Acids. *J. Chem. Phys.* **2018**, *148*, No. 134309.
(52) Van Hoozen, B. L.; Petersen, P. B. A Combined Electronic Structure and Molecular Dynamics Approach to Computing the OH Vibrational Feature of Strongly Hydrogen-Bonded Carboxylic Acids. *J. Chem. Phys.* **2017**, *147*, No. 224304.
(53) Tian, Z. X.; Kass, S. R. Does Electrospray Ionization Produce Gas-Phase or Liquid-Phase Structures? *J. Am. Chem. Soc.* **2008**, *130*, 10842−10843.
(54) Schröder, D.; Budesinsky, M.; Roithova, J. Deprotonation of *p*-Hydroxybenzoic Acid: Does Electrospray Ionization Sample Solution or Gas-Phase Structures? *J. Am. Chem. Soc.* **2012**, *134*, 15897−15905.
(55) Patrick, A. L.; Cismesia, A. P.; Tesler, L. F.; Polfer, N. C. Effects of ESI Conditions on Kinetic Trapping of the Solution-Phase Protonation Isomer of *p*-Aminobenzoic Acid in the Gas Phase. *Int. J. Mass Spectrom.* **2017**, *418*, 148−155.

https://doi.org/10.1021/acs.jpca.1c05879
J. Phys. Chem. A 2021, 125, 9288−9297